Mixed Representation RPA Calculation for Octupole Excitations on Superdeformed Sates in the ^{40}Ca and Neutron-Rich Sulfur Regions

T. Inakura,[a] H. Imagawa,[b] Y. Hashimoto,[b]
S. Mizutori,[c] M. Yamagami,[d] and K. Matsuyanagi[e]

[a] *Graduate School of Science and Technology, Niigata University, Niigata 950-2181, Japan*

[b] *Institute of Physics, University of Tsukuba, Ibaraki 305-8571, Japan*

[c] *Department of Human Science, Kansai Women's College, Osaka 582-0026, Japan*

[d] *Radioactive Isotope Physics Laboratory, RIKEN, Saitama 351-0198, Japan*

[e] *Department of Physics, Graduate School of Science, Kyoto University, Kyoto 606-8502, Japan*

December 15, 2005

Abstract

By means of the mixed representation RPA based on the Skyrme-Hartree-Fock mean field, we investigate low-frequency octupole excitations built on the superdeformed (SD) states in the $N = Z$ nuclei around ^{40}Ca and the neutron-rich Sulfur isotopes. The RPA calculation is carried out fully self-consistently on the three-dimensional Cartesian mesh in a box, and yields a number of low-frequency octupole vibrations built on the SD states in ^{32}S, ^{36}Ar, ^{40}Ca and ^{44}Ti. In particular, a strongly collective $K^\pi = 1^-$ octupole vibration is suggested to appear on top of the SD state in ^{40}Ca. For ^{48,50}S close to the neutron drip line, we find that the low-lying state created by the excitation of a single neutron from a loosely bound low Ω level to a high Ω resonance level acquires an extremely strong octupole transition strength due to the spatially very extended structure of the particle-hole wave functions.

1 Introduction

Nowadays, more than two hundreds superdeformed (SD) bands are identified in various mass (A=60, 80, 130, 150, 190) regions [1–6]. Every SD regions have their own characteristics so that we can significantly enlarge and deepen our understanding of nuclear structure by systematically investigating similarities and differences among the SD bands in different mass region. The SD shell structure is significantly different from that of normal deformation. Namely, each major shell at the SD shape consists of about equal numbers of positive- and negative-parity levels. This is a favourable situation for the appearance of negative-parity collective modes. In fact, various mean-field calculations [7–9] and quasiparticle random phase approximation (RPA) [10,11] on the basis of the rotating mean field (cranked shell model) indicated that SD nuclei are very soft against both the axial and non-axial octupole deformations. Thus, low-frequency octupole vibrations have been predicted

to appear near the SD yrast lines [12], and recently discovered in experiments for heavy SD nuclei in the Hg-Pb region [13], and also in ^{152}Dy [14].

In recent years, the SD bands have been discovered also in the ^{40}Ca region: In ^{36}Ar the SD band has been identified up to its termination at $I^\pi = 16^+$ [15–17]. The SD band in the spherical doubly magic nucleus ^{40}Ca is built on the 8p-8h excited 0^+ state at 5.213 MeV [18, 19]. The SD shell gap at $N = 20$ ($Z = 20$) is associated with the neutron (proton) 4p-4h excitation from below the $N = 20$ ($Z = 20$) spherical closed shell to the $f_{7/2}$ shell. The rotational band built on the excited 0^+ state at 1.905 MeV in ^{44}Ti may also be regarded as belonging to a family of the SD band [20]. The fact that rotational bands built on excited 0^+ states are systematically observed is a unique feature of the SD bands in the ^{40}Ca region, considering that the low angular momentum portions of the SD bands in heavy nuclei are unknown in almost all cases (except the fission isomers). We have confirmed that the symmetry-unrestricted Skyrme-Hartree-Fock (SHF) calculation indeed yields the SD local minima corresponding to these experimental data [21]. It should be stressed that, in spite of the remarkable progress in experiment, the doubly magic SD band in ^{32}S associated with the SD magic number N=Z=16, which has been anticipated quite a long time [22–31], has not yet been observed and remains as a great challenge.

If we believe that Z=16 is a good SD magic number, the existence of the SD shell gap at $N = 20$, revealed by the discovery of the SD band in ^{40}Ca [18], suggests that another SD band would appear in the neutron-rich nucleus ^{36}S. Furthermore, combining with the fact that the SD bands have been observed in ^{60,62}Zn [32, 33], we can expect that Sulfur isotopes around ^{48}S, which are situated close to the neutron-drip line [34, 35], constitute a new SD region associated with the SD shell gaps at $Z = 16$ and $N \simeq 32$. In fact, the symmetry-unrestricted SHF calculation [36] yields the SD local minima for ^{48,50}S as well as ^{32}S.

The investigation of low-frequency octupole vibrations built on the SD states in the A=30-50 region possesses some new features that are absent in the study of heavy SD nuclei. For the $N = Z$ nuclei in the ^{40}Ca region, it may be possible to observe in experiment such collective modes built on the known SD 0^+ states. Moreover, because the proton and neutron shell structures are essentially the same, we can expect that strong coherence takes place between the proton and neutron excitations and brings about an enhanced collectivity of these modes. Concerning the anticipated new SD region around ^{48}S, we will encounter an essentially new situation: Because these nuclei are situated close to the neutron drip line, there is almost no bound state above the Fermi surface and nucleons may excite into the continuum states even in the lowest excited states.

The study of soft collective modes unique to unstable nuclei close to the neutron drip line is one of the current major subjects in nuclear structure physics. For this purpose, the continuum RPA [37, 38] based on the Green's function method correctly treating the continuum boundary condition has been widely used (see, e.g., [39, 40]). Recently, this method has been extended [41–43] to include the pairing correlations on the basis of the Hartree-Fock-Bogoluibov theory. It is called the continuum quasiparticle-RPA (QRPA). Furthermore, a new technique of solving the QRPA equations using the canonical basis has been developed [44]. The canonical basis has also been used in the QRPA calculation based on the relativistic mean field scheme [45, 46]. A serious limitation of these works is that, because the construction of the Green's function for deformed mean fields is difficult, they are restricted to spherical nuclei. Quite recently, however, this limitation has been overcome by Nakatsukasa and Yabana [47]; they have proposed an iterative method of constructing the response functions for deformed systems with the proper boundary condition in the

three-dimensional (3D) coordinate space. They have also proposed a feasible method of treating the continuum boundary condition by means of the real-space time-dependent HF approach with the absorbing boundary condition.

In this paper, we investigate low-frequency octupole excitations built on the SD states in neutron rich Sulfur isotopes as well as those in the ^{40}Ca region. For this purpose, we employ the mixed representation RPA [48–50] based on the SHF mean field. In this RPA scheme, the *particles* above the Fermi surface are described in the coordinate representation, while the *holes* are represented in the HF single-particle basis. The RPA calculation is carried out fully self-consistently on the 3D Cartesian mesh in a box. The major advantage of this approach is that it is a fully self-consistent scheme in the sense that the same effective interaction is used in both the mean field and the RPA calculations; i.e., all terms of the Skyrme interaction contributing to the RPA equations of motion are taken into account. It should be stressed here that such a fully self-consistent calculation using the Skyrme-type interaction is difficult in the Green's function approach, so that, usually, the residual particle-hole interactions associated with the spin-orbit and Coulomb interactions, as well as those associated with the time-odd components (related to the spin and current densities) of the mean field, are ignored in the continuum RPA based on the SHF mean field. Another important merit of our approach is that, thanks to the use of the 3D Cartesian mesh representation, we can treat strongly deformed nuclei on the same footing as spherical nuclei. Furthermore, because the *particles* are described in the coordinate representation, we do not need to introduce an upper cut off for their energies. Quite recently, Imagawa and Hashimoto constructed a new computer code that carries out the fully self-consistent RPA calculation in the mixed representation on the basis of the SHF mean field, and they carefully tested its numerical accuracy [51–53]. The numerical calculations of this paper were carried out using a refined version this code.

This paper is organized as follows: In Section 2, a brief account of the self-consistent RPA calculation using the mixed representation is given. In Section 3, we present and discuss the results of numerical calculation for low-frequency octupole vibrations built on the SD states in $N = Z$ nuclei, ^{32}S, ^{36}Ar, ^{40}Ca, and ^{44}Ti. In Section 4, the results for neutron-rich Sulfur isotopes, ^{36}S, ^{48}S, and ^{50}S, are presented and discussed. The main results of this paper are summarized in Section 5.

A preliminary version of this work was reported in Refs. [54, 55].

2 RPA calculation using the mixed representation

2.1 Basic formulae

The RPA equations in the mixed representation are easily derived either by means of the lineralized equations of motion approach [48] or the small-amplitude approximation of the time-dependent HF theory [49]. Here, we recapitulate the basic formula following the former approach.

The creation and annihilation operators of nucleon, $\psi^\dagger(x)$ and $\psi(x)$, are divided into those for the bound states and those for the continuum states:

$$\psi^\dagger(x) = \sum_\alpha \varphi^*_\alpha(x) c^\dagger_\alpha + \int_0^\infty \mathrm{d}\varepsilon \varphi^*_\varepsilon(x) c^\dagger_\varepsilon, \tag{1}$$

$$\psi(x) = \sum_\alpha \varphi_\alpha(x) c_\alpha + \int_0^\infty \mathrm{d}\varepsilon \varphi_\varepsilon(x) c_\varepsilon, \tag{2}$$

where x denotes a set of space, spin and isospin coordinates, i.e., $x = \{\boldsymbol{r}, \sigma, \tau\}$. The symbol α denotes the HF bound states with wave functions $\varphi_\alpha(x)$, while the energy ε specifies the continuum states with wave functions $\varphi_\varepsilon(x)$. With the use of the *particle* and *hole* concepts, we then divide the nucleon operators according to the occupation number θ_α in the HF ground state ($\theta_\alpha = 0$ for unoccupied states, $\theta_\alpha = 1$ for occupied states). We consider even-even nuclei and assume that the single-particle states α and their time reversed states are doubly degenerated. Obviously, the continuum states belong to the particle space. On the other hand, for the bound states, the operators ($c^\dagger_\alpha$, c_α) are divided into the particle operators ($a^\dagger_m$, a_m) and the hole operators ($b^\dagger_i$, b_i),

$$c^\dagger_\alpha = (1-\theta_\alpha)a^\dagger_m + \theta_\alpha b_i, \tag{3}$$
$$c_\alpha = (1-\theta_\alpha)a_m + \theta_\alpha b^\dagger_i, \tag{4}$$

where the indices m and i are used in place of α to distinguish the particle and hole states. Thus, the particle creation and annihilation operators, $a^\dagger(x)$ and $a(x)$, at the coordinate x are written in terms of the above ($a^\dagger_m$, a_m) and the integration with respect to the positive energy ε specifying the continuum states;

$$a^\dagger(x) = \sum_m \varphi^*_m(x)a^\dagger_m + \int \mathrm{d}\varepsilon \varphi^*_\varepsilon(x)a^\dagger_\varepsilon, \tag{5}$$
$$a(x) = \sum_m \varphi_m(x)a_m + \int \mathrm{d}\varepsilon \varphi_\varepsilon(x)a_\varepsilon. \tag{6}$$

In the mixed representation, the coordinate representation is used for particles, while the HF basis specified by the discrete index i are used for holes. Thus, the following expressions of the nucleon operators are convenient:

$$\psi^\dagger(x) = a^\dagger(x) + \sum_i \varphi^*_i(x)b_i, \tag{7}$$
$$\psi(x) = a(x) + \sum_i \varphi_i(x)b^\dagger_i. \tag{8}$$

Note that

$$\{a(x), a^\dagger(x')\} = P(x,x') = \delta(x,x') - Q(x,x') \equiv \delta(x,x') - \sum_i \varphi_i(x)\varphi^*_i(x'), \tag{9}$$

where $P(x,x')$ and $Q(x,x')$ are the projectors onto the particle and hole spaces, respectively.

Using an abbreviation, $\sum_x \equiv \sum_{\sigma\tau}\int \mathrm{d}\boldsymbol{r}$, the RPA phonon creation operators in the mixed representation are written as

$$O^\dagger_\lambda = \sum_i \sum_x \left\{ X^\lambda_i(x)a^\dagger(x)b^\dagger_i - Y^\lambda_i(x)b_i a(x) \right\}. \tag{10}$$

Then, the RPA eigenvalue equations determining the eigen-energies, $\hbar\omega_\lambda$, and the forward and backward amplitudes, $X^\lambda_i(x)$ and $Y^\lambda_i(x)$ are given in the following form:

$$\sum_j \sum_{x'} \left[A_{ij}(x,x')X^\lambda_j(x') + B_{ij}(x,x')Y^\lambda_j(x') \right] = \hbar\omega_\lambda X^\lambda_i(x) \tag{11}$$
$$\sum_j \sum_{x'} \left[B^*_{ij}(x,x')X^\lambda_j(x') + A^*_{ij}(x,x')Y^\lambda_j(x') \right] = -\hbar\omega_\lambda Y^\lambda_i(x), \tag{12}$$

where

$$A_{ij}(x,x') = \sum_{x'',x'''} P(x,x'')\tilde{A}_{ij}(x'',x''')P(x''',x'), \tag{13}$$

$$B_{ij}(x,x') = \sum_{x'',x'''} P(x,x'')\tilde{B}_{ij}(x'',x''')Q(x''',x'), \tag{14}$$

and

$$\tilde{A}_{ij}(x,x') = [h_{\rm HF}(x,x') - e_i\delta(x,x')]\,\delta_{ij} + \sum_{x''x'''} \varphi_i(x'')\varphi_j^*(x''')\frac{\partial^2 E[\rho]}{\partial\rho(x'',x)\partial\rho(x',x''')}, \tag{15}$$

$$\tilde{B}_{ij}(x,x') = \sum_{x''x'''} \varphi_i(x'')\varphi_j(x''')\frac{\partial^2 E[\rho]}{\partial\rho(x'',x)\partial\rho(x''',x')}. \tag{16}$$

The above RPA equations can be recast into the following form for the linear combinations, $\phi_i^{(\pm)\lambda}(x) = X_i^\lambda(x) \pm Y_i^{\lambda *}(x)$:

$$\sum_{x'} [h_{\rm HF}(x,x') - e_i\delta(x,x')]\,\phi_i^{(+)\lambda}(x') + \sum_{x'x''} P(x,x')h_{\rm RPA}^{(+)\lambda}(x',x'')\varphi_i(x'') = \hbar\omega_\lambda\phi_i^{(-)\lambda}(x)\ , \tag{17}$$

$$\sum_{x'} [h_{\rm HF}(x,x') - e_i\delta(x,x')]\,\phi_i^{(-)\lambda}(x') + \sum_{x'x''} P(x,x')h_{\rm RPA}^{(-)\lambda}(x',x'')\varphi_i(x'') = \hbar\omega_\lambda\phi_i^{(+)\lambda}(x)\ . \tag{18}$$

Here, the RPA Hamiltonian is given by

$$h_{\rm RPA}^{(\pm)\lambda}(x,x') = \sum_{x'',x'''} \rho^{(\pm)\lambda}(x'',x''')\frac{\delta h_{\rm HF}(x,x')}{\delta\rho(x'',x''')}, \tag{19}$$

where

$$\rho^{(\pm)\lambda}(x,x') = \sum_i \left[\varphi_i^*(x')\phi_i^{(\pm)\lambda}(x) \pm \phi_i^{(\pm)\lambda *}(x')\varphi_i(x)\right]. \tag{20}$$

represents the transition density. The above equations are obtained also by making the small-amplitude approximation for the equations of motion of the time-dependent HF mean field [49]. The explicit expression of $h_{\rm RPA}^{(\pm)\lambda}(x,x')$ is given in Appendix. The transition matrix elements for the octupole operators Q_{3K} are given by

$$\langle 0|Q_{3K}|\lambda\rangle = \sum_x Q_{3K}(\boldsymbol{r}) \sum_i \left[X_i^\lambda(x)\varphi_i^*(x) + \varphi_i(x)Y_i^\lambda(x)\right].$$

2.2 Details of numerical calculation

We solve the SHF equation on the 3D Cartesian mesh assuming the reflection symmetry about the (x,y)-, (y,z)-, and (z,x)-planes. The derivative operators are treated by means of the Lagrange mesh method [56], except for the derivative of the Coulomb potential for which the finite difference method with the 9 points formula is used. Based on the numerical test explained below, we adopt the mesh spacing $\Delta x = 0.6$ fm. Because we treat the superdeformed nuclei, we use the rectangular box with 15 and 25 mesh points in the positive directions of the minor and major axes, respectively, i.e., we take the mesh points at $x = 0.3, 0.9, ..., 8.7$ fm, $y = 0.3, 0.9, ..., 8.7$ fm and $z = 0.3, 0.9, ..., 14.7$ fm (the major axis is called the z-axis). Considering the reflection symmetries, the total size of the box is thus

$17.4 \times 17.4 \times 29.4$ fm^3. For the effective interaction, the standard versions of the Skyrme interaction, SIII [57], SkM* [58] and SLy4 [59], are used.

We then solve the RPA equations, (17) and (18), using the SHF solutions obtained above. With the mesh discretization, Eqs. (17) and (18) become the matrix eigenvalue problem with the $2 \times N_h \times N_p$ dimension, where N_h and N_p denote the numbers of the hole states and the mesh points, respectively. Because we assume the reflection symmetry about the three planes, the RPA eigen-value equations are separated into four blocks specified by the parity quantum numbers. It is easily ascertained that the negative parity operators are classified into the four groups, $(-,+,+)$, $(+,-,+)$, $(+,+,-)$, and $(-,-,-)$, where the first, the second, and the third signs indicate the parity with respect to the reflection about the (y,z)-, (z,x)-, and (x,y)-planes, respectively. For instance, the octupole operator $Q_{30} = r^3 Y_{30}$ belongs to the $(+,+,-)$ sector. On the other hand, the octupole operators with $K \neq 0$, $Q_{3K}^{(\pm)} = r^3 \left(Y_{3K} \pm Y_{3,-K}\right)/\sqrt{2}$, are classified according to the parity quantum numbers as shown in Table 1. We calculate the eigenvalues and eigenvectors of the RPA matrix by means of the conjugate gradient method in a version developed in Refs. [51–53].

It should be noted here that the translational symmetry is broken in the coordinate mesh representation so that the eigenvalues of the RPA corresponding to the spurious center of mass motion do not necessarily become zero. It is possible that the eigenvalue $\hbar\omega_\lambda$ corresponding to the spurious mode become pure imaginary. Moreover, in deformed nuclei, except for the $(-,-,-)$ sector, these spurious modes can mix with the octupole modes having the same symmetry properties (see Table 1 for the classification of the dipole operators corresponding to the center of mass motion). It is therefore very important to carefully check the accuracy of numerical calculation whether or not the spurious center of motions are decoupled from the physical excitations in a good approximation. In the numerical calculation, we manipulate this problem with the following procedure. Combining Eqs. (11) and (12), the RPA eigenvalue problem is transformed into the following form:

$$\begin{aligned}\sum_{jk}\sum_{x',x''}[A_{ij}(x,x')A_{jk}(x',x'') &- A_{ij}(x,x')B_{jk}(x',x'') \\ +B_{ij}(x,x')A_{jk}(x',x'') &- B_{ij}(x,x')B_{jk}(x',x'')]\phi_k^{(-)\lambda}(x'') = (\hbar\omega_\lambda)^2\phi_i^{(-)\lambda}(x). \quad (21)\end{aligned}$$

This form is convenient for applying the conjugate gradient method which is valid only for real eigenvalues, because, when the eigenvalue $\hbar\omega_\lambda$ of the spurious mode take an imaginary value, we can easily identify it as a negative $(\hbar\omega_\lambda)^2$ solution of this equation. The result of such an accuracy test of numerical calculation is presented in Fig. 1. In this figure, low-energy solutions of the above RPA equation for negative-parity excitations on the SD ground state in ^{40}Ca are plotted as functions of the mesh spacing Δx used in the SHF-RPA calculation with the SIII interaction. We see that a good convergence is attained at about $\Delta x = 0.6$ fm, although excitation energies of the spurious center of mass modes fluctuate in the region of $\Delta x > 0.7$ fm. It should be noted that the excitation energies of the physical excitation modes and their transition strengths almost converge for $\Delta x < 0.7$ fm. Thus, we adopt $\Delta x = 0.6$ fm in the numerical calculations presented below. We note that the use of this mesh spacing corresponds the introduction of an effective energy cut-off $E_{\rm cut-off} = (\hbar^2/2m)(\pi/\Delta x)^2 \sim 500$ MeV. This value is sufficiently large. Accordingly, it may be allowed to say that our calculation is, in practice, cut-off free. Certainly, it is desirable to use a smaller Δx and a larger box for better numerical accuracy, but it is difficult to do so with the available computing power at the present time. This limitation will be overcome in the near future.

In presenting the results of the SHF-RPA calculation in the subsequent sections, we label the SHF single-particle levels in terms of the asymptotic quantum numbers $[N_{\rm osc}, n_z, \Lambda, \Omega]$ for the modified oscillator potential. It should be noted that this labeling is used solely for convenience of presentation, and do not always mean that they are good quantum numbers. The labeling of the SHF single-particle states is done by examining their properties, like reflection symmetries and expectation values of the angular momentum, and by comparison with the single-particle level scheme obtained in Ref. [60], where the deformed Woods-Saxon potential simulating the SHF potential was constructed and properties of both the bound states and the discretized continuum states for this potential are analysed in detail. In this reference, the RPA calculations were also carried out for the octupole excitations on the SD states under consideration, using the conventional matrix formulation with these single-particle levels in a truncated model space and a density dependent contact interaction. The results of this simple RPA calculation qualitatively agree with the results of the mixed representation RPA calculation presented below. Thus, we have used the correspondence between the two calculations for checking the numerical calculation. As we shall discuss later, this comparison was especially useful for the purpose of distinguishing the resonant levels from the non-resonant discretized continuum levels.

3 Results of calculation for the ^{40}Ca region

Figure 2 displays the transition strength distributions obtained by the SHF-RPA calculation with the SIII interaction for low-frequency octupole excitations built on the SD states in ^{32}S, ^{36}Ar, and ^{40}Ca. The RPA transition stengths $B(Q^{\rm IS}3)$ are here defined as the squared matrix elements of the isoscalar octupole operators between the SD excited state $|\lambda\rangle$ and the SD ground state $|0\rangle$, $B(Q^{\rm IS}3) = |\langle 0|Q^{\pi}_{3K}+Q^{\nu}_{3K}|\lambda\rangle|^2$. In this figure, the RPA transition strengths for the electric octupole operators, $B(E3) = |\langle 0|Q^{\pi}_{3K}|\lambda\rangle|^2$, are also indicated for levels possessing strong collectivity. Here, Q^{π}_{3K} and Q^{ν}_{3K} denote the proton and neutron octupole operators. It should be noted that these quantities represent the intrinsic matrix elements squared. Accordingly, in order to evaluate the reduced transition probabilities in the laboratory frame, appropriate Clebsch-Gordan (CG) coefficients squared and other kinematical factors should be multiplied to them [61]. Specifically, for the transition from the 3^- member of the $K = 0$ ($K \neq 0$) band to the SD 0^+ band head, the CG coefficient is unity and the kinematical factor is 1/7 (2/7). The SHF calculation for ^{40}Ca in fact yields a SD mean field with small triaxially of γ=7°, while the SD solutions for ^{32}S and ^{36}Ar are axially symmetric. Nevertheless, for simplicity, we here present the result of the RPA calculation on the basis of the SHF mean field obtained under the constraint γ=0°. The effect of the small triaxial deformation on these excitation modes will be discussed in the end of this section.

For ^{32}S, we obtain a low-frequency collective $K^{\pi} = 2^-$ mode at 2.6 MeV above the SD band head. It possesses a large isoscalar octupole transition strength of 30 W.u. (1 W.u. $\simeq$ 61 fm^6 for ^{32}S). The unperturbed strengths in the 3.5 MeV region, seen in Fig. 2, are associated with the proton and neutron excitations from the $[211\frac{1}{2}]$ level to the $[321\frac{3}{2}]$ level. The RPA transition strength is greatly enhanced in comparison with the unperturbed strengths and the RPA eigen-energy is significantly shifted down from the unperturbed particle-hole excitation energies, so that this $K^{\pi} = 2^-$ mode can be regarded as a collective octupole vibration.

For ^{36}Ar, we obtain two strongly collective modes; a $K^{\pi} = 2^-$ mode at 3.9 MeV and

a $K^\pi = 1^-$ mode at 4.0 MeV. They possess large isoscalar octupole transition strengths of 27 and 25 W.u., respectively (1 W.u. $\simeq$ 77 fm^6 for ^{36}Ar). This 2^- mode is similar to that in ^{32}S discussed above, except for the following difference: Because the quadrupole deformation of the SD state in ^{36}Ar is smaller ($\beta_2 = 0.51$) than that in ^{32}S ($\beta_2 = 0.72$), the unperturbed particle-hole excitation energies (4.9-5.0 MeV) of protons and neutrons from the up-sloping $[211\frac{1}{2}]$ level to the down-sloping $[321\frac{3}{2}]$ level are larger in ^{36}Ar than in ^{32}S. Accordingly, the RPA excitation energy of the 2^- mode in ^{36}Ar is higher than that in ^{32}S. Concerning the 1^- mode, its excitation energy is considerably shifted down from the particle-hole excitation energies (4.6-4.9 MeV) of protons and neutrons from the $[202\frac{5}{2}]$ level to the $[321\frac{3}{2}]$ level. Considering this together with the enhanced transition strength, this 1^- mode can also be regarded as a mode possessing strongly collectivity. In addition to the 2^- and 1^- modes mentioned above, we also obtain a 0^- mode and another 1^- mode in the 2.8-2.9 MeV region, which are moderately collective.

For ^{40}Ca, we obtain a low-frequency collective $K^\pi = 1^-$ mode at about 1.2 MeV. It possesses a large isoscalar octupole transition strengths of 29 W.u. (1 W.u. $\simeq$ 95 fm^6 for ^{40}Ca). The unperturbed particle-hole strengths in the 2.2 MeV region are associated with the proton and neutron excitations from the $[321\frac{3}{2}]$ level to the $[200\frac{1}{2}]$ level. The fact that the RPA transition strength is significantly enhanced in comparison with the unperturbed strength and the RPA eigen-energy is shifted down from the unperturbed particle-hole excitation energies indicates that this $K^\pi = 1^-$ mode possesses a strong collectivity. We also obtained a strongly collective $K^\pi = 0^-$ mode possessing quite large strength (82 W.u.) at about 3.3 MeV. For this $K^\pi = 0^-$ transitions, although small unperturbed strengths (about 0.1 W.u.) associated with the particle-hole excitations of protons and neutrons from the $[321\frac{3}{2}]$ level to the $[202\frac{3}{2}]$ level are seen at about 4.6 MeV, their strengths are small mainly because they strongly violate the asymptotic selection rule for low-energy octupole transitions in the SD harmonic-oscillator potential [11]. Thus, this collective $K^\pi = 0^-$ mode is generated mainly from many particle-hole configurations lying in the energy region higher than that shown in this figure. We mention that these collective modes in ^{40}Ca were previously reported by one of authors (H.I.) in Ref. [51].

For all the RPA eigen-modes presented in Fig. 2, we can say the followings:
1) The approximate relation, $B(Q^{\rm IS}3) \approx 4B(E3)$, holds, indicating that they are collective modes generated by coherent superposition of proton and neutron excitations.
2) The RPA strengths are greatly enhanced from the unperturbed strengths of individual particle-hole excitations. This indicates that these RPA eigen-modes are generated by collective contributions of quite a number of particle-hole excitations.
The role of coherence between the neutron and proton excitations in building up these collective enhancements can also be seen by comparing these RPA transition strengths for the $N = Z$ nuclei, ^{32}S and ^{40}Ca, with those for the $N \neq Z$ nucleus ^{36}S presented in the succeeding section.

We also carried out the same kind of calculation using the SkM* [58] and the SLy4 [59] interactions. The results for strongly collective excitations of these SHF-RPA calculations with different versions of the Skyrme interaction are compared in Fig. 3. Note that the calculations for ^{40}Ca were done with the constraint γ=0° for the mean fields, although the SHF calculations yield small triaxial deformations; 4° and 8° with the SkM* and SLy4 interactions, respectively. For all excitation modes discussed above, we obtained the results qualitatively similar to those with the SIII interaction, Namely, our prediction about the existence of these collective modes is rather robust, depending little on the choice of the Skyrme interaction.

Next, let us examine the effects of the triaxial deformations of the SD mean field on the RPA eigen-modes discussed above. Figure 4 shows the strongly collective excitations in ^{40}Ca and ^{44}Ti, obtained by the RPA calculation taking into account the triaxiality of the SD mean fields. Because K is not a good quantum number due to the K mixing, the K values denoted on the right-hand sides of individual levels indicate the maximum components, and the transition strengths for these K values are indicated beside the arrows in this figure. A clear consequence of the triaxiality is that the $K \neq 0$ modes split into doublets. This qualitative feature is common to the RPA calculations with the SIII, SkM* and SLy4 interactions. Concerning the ^{40}Ca case, however, the small triaxilality ($\gamma < 10^\circ$) in the HF mean field might be easily diminished by, e.g., the zero-point fluctuation in the γ direction and/or pairing correlations. Therefore, it is not clear whether this splitting of the 1^- mode is important or not. On the other hand, the triaxial deformations for ^{44}Ti, obtained in the SHF calculations with the SIII and SLy4 interactions, are significantly larger than those for ^{40}Ca (see the γ values indicated at the bottom of Fig. 4). In such cases, it may be interesting to examine the theoretical calculation against possible experimental signatures of the triaxility. For instance, the calculation with the SIII interaction yields a "$K^\pi = 0^-$" collective mode at 2.4 MeV and a "$K^\pi = 2^-$" doublet at 3.0 and 3.5 MeV, which possess large isoscalar octupole transition strengths of 27, 24 and 16 W.u., respectively (1 W.u. $\simeq$ 115 fm^6 for ^{44}Ti). In addition, we also obtain another 0^- mode at 5.3 MeV, two 1^- doublets at 2.5 and 4.2 MeV, and another 2^- doublet at 3.2 MeV, which are moderately collective (not shown in Fig. 4 but displayed in Fig. 5).

The RPA transition strengths are compared with the unperturbed particle-hole strengths in Fig. 5. For the $K = 0$ transitions, small unperturbed strengths (about 0.15 W.u.) associated with the particle-hole excitations of protons and neutrons from the $[321\frac{3}{2}]$ level to the $[202\frac{3}{2}]$ level are seen at about 3.2 MeV. For the $K = 2$ transitions, the peaks in the 4.1-4.3 MeV region in the unperturbed strengths are associated with the particle-hole excitations of protons and neutrons from the $[200\frac{1}{2}]$ level to the $[312\frac{5}{2}]$ level. These "$K^\pi = 0^-$" and "$K^\pi = 2^-$" RPA modes are generated by collective superpositions of not only these relatively low-lying configurations but also many particle-hole configurations lying in the higher energy region. Thus, the present RPA calculation suggests that the appearance of the 2^- doublet may serve as a good indicator of the triaxial nature of the SD state of ^{44}Ti. Experimental search for such a doublet on top of the SD band head seems very interesting.

4 Results of calculation for the neutron-rich Sulfur region

Figure 6 displays the transition strength distributions obtained by the SHF-RPA calculation with the SIII interaction for low-frequency octupole excitations built on the SD states in ^{36,48,50}S. Let us first discuss the result of calculation for the neutron-rich ^{36}S. For this nucleus, we obtain a $K^\pi = 1^-$ mode at 2.6 MeV and a $K^\pi = 2^-$ mode at 4.2 MeV. As they possess the isoscalar octupole transition strengths of 13 W.u. and 16 W.u., respectively, they are moderately collective (1 W.u. $\simeq$ 77 fm^6 for ^{36}S). It is interesting to compare this result with those for ^{32}S and ^{40}Ca discussed in the previous section. The 1^- mode in this nucleus is similar to the 1^- mode in ^{40}Ca, but its transition strength is less than half of the latter. This reduction of the collectivity is understood in terms of the weakening of the coherence between the proton and neutron excitations when one goes from the $N = Z$ nucleus to the $N \neq Z$ nucleus. Looking into the microscopic details, we find that, for example, the

particle-hole excitations of protons and neutrons from the $[321\frac{3}{2}]$ level to the $[200\frac{1}{2}]$ level act coherently to produce the $K^\pi = 1^-$ collective mode in ^{40}Ca, but this proton excitation is absent in the case of ^{36}S because the $[321\frac{3}{2}]$ level is unoccupied. Analogous argument also applies to the $K^\pi = 2^-$ mode. This mode is similar to the 2^- mode in ^{32}S, but, its transition strength is about half of the latter. This is understood again in terms of the weakening of the coherence between the proton and neutron excitations. For instance, the particle-hole excitations of protons and neutrons from the $[211\frac{1}{2}]$ level to the $[321\frac{3}{2}]$ level act coherently to produce the $K^\pi = 2^-$ collective mode in ^{32}S, but this neutron excitation is absent in the case of ^{36}S because the $[321\frac{3}{2}]$ level is already occupied.

Next, let us discuss the result of calculation for ^{48}S and ^{50}S close to the neutron-drip line. For ^{48}S, we obtain a $K^\pi = 1^-$ mode at very low excitation energy, 0.51 MeV. This mode possesses a large octupole transition strength of 31 W.u. (1 W.u. $\simeq$ 137 fm^6 for ^{48}S). The RPA eigen-energy is shifted down only slightly (0.14 MeV) from the unperturbed energy (0.65 MeV) of the neutron excitation from the $[431\frac{1}{2}]$ level to the $[310\frac{1}{2}]$ level. The unperturbed transition strength for this single-particle excitation is extremely large, i.e., $B(Q^{\rm IS}3) = 7.7$ W.u. The major cause of this remarkable strength is understood as follows: Both the $[431\frac{1}{2}]$ and $[310\frac{1}{2}]$ levels are loosely bound with binding energy about 2 MeV. Because, as is well known, wave functions of the loosely bound states are significantly extended outside of the half-density radius, the matrix element of the octupole operator between these configurations acquires a large contribution from the region outside of the nuclear surface. Thus, such a transition strength can become very large in nuclei close to the neutron drip. Although the increase of the RPA transition strength from the unperturbed strength indicates the presence of collective effects, it may be appropriate to consider that the major character of this mode is of single-particle-type. In contrast to the low energy peak at 0.51 MeV discussed above, the peaks above the neutron-emission threshold (indicated by arrows in Fig. 6) are considered to be associated with the excitations to discretized non-resonant continuum states. We examined that these peaks in the continuum indeed moves when we increase the box size in the numerical calculation. Therefore, we cannot give definite physical meanings to these peaks.

For ^{50}S, we obtain a $K^\pi = 2^-$ mode at 2.5 MeV. Like the $K^\pi = 1^-$ mode in ^{48}S, it is essentially a single-particle-type excitation, although it has extremely large octupole transition strength, 55 W.u. (1 W.u. $\simeq$ 149 fm^6 for ^{50}S). Namely, it is created mainly by the neutron excitation from the loosely bound $[310\frac{1}{2}]$ level to the resonance $[422\frac{5}{2}]$ level. The RPA eigen-energy of this mode is shifted down only slightly (0.5 MeV) from the unperturbed excitation energy (3.0 MeV) of this particle-hole configuration. Because the resonance $[422\frac{5}{2}]$ level is situated near the centrifugal barrier top, its wave function is significantly extended far out side of the half-density radius of this nucleus. Thus, the unperturbed octupole transition strength for this particle-hole excitation takes an extremely large value, $B(Q^{\rm IS}3) = 22$ W.u. This resonance interpretation of the $[422\frac{5}{2}]$ level is largely based on the analysis made in Ref. [60] where the deformed Woods-Saxon potential simulating our SHF potential was constructed and properties of the discretized continuum states for this potential are analysed in detail. It was then found that the energy and the root-mean-square radius of this level were stable against the variation of the box size. In the same paper, this conclusion was confirmed also by carrying out the eigenphase analysis for this level. The appearance of this resonance level is easily understood as due to the rather high centrifugal barrier for the relatively large value of the symmetry axis component of the angular momentum, $\Omega = 5/2$. We confirmed that this 2^- peak at 2.5 MeV does not move but the other peaks moves when we increase the box size in the numerical calculation.

Thus, like in ^{48}S, except for the 2^- peak, the peaks above the the neutron-emission threshold are considered to be associated with the excitations to discretized non-resonant continuum states.

We also carried out the same kind of calculation using the SkM* [58] and the SLy4 [59] interactions. The results of calculations with different versions of the Skyrme interaction are compared in Fig. 7. For the SLy4 interaction, the SD local minimum does not appear in ^{48}S, so that the RPA calculation was not done for this nucleus. Except for this, these Skyrme interactions yield qualitatively similar results for the $K^\pi = 1^-$ and $K^\pi = 2^-$ modes.

To accurately describe the spatially extended wave functions, like the loosely bound levels and resonance levels in ^{48}S and ^{50}S discussed above, it is certainly desirable to use a bigger box in the numerical calculation. Although it is difficult to significantly enlarge the box size under the present situation of computing power, we plan to manipulate this problem by incorporating the adaptive coordinate method into our scheme of numerical calculation. We believe, however, that the qualitative features of the present RPA calculation will remain valid. We have not obtained well-developed collective octupole modes for ^{48}S and ^{50}S. In such unstable nuclei close to the neutron-drip line, there is almost no bound state above the Fermi surface and neutrons are excited to the continuum states. It seems difficult to develop collective correlations among different particle-hole configurations under such situations. Quite recently, however, one of the authors (M. Y.) pointed out that the pairing correlations play an important role for the emergence of low-frequency collective modes in such drip-line nuclei [62]. For studying such pairing effects for collective excitations, it will be interesting to extend the mixed representation RPA based on the SHF mean field to that based on the SHF-Bogoliubov mean field.

5 Conclusions

By means of the mixed representation RPA based on the SHF mean field, we have investigated low-frequency octupole excitations on the SD states in the $N = Z$ nuclei around ^{40}Ca and the neutron-rich Sulfur isotopes. The RPA calculation has been carried out on the 3D Cartesian mesh in a box, and yielded a number of low-frequency octupole vibrations built on the SD states in ^{32}S, ^{36}Ar, ^{40}Ca and ^{44}Ti. In particular, a strongly collective $K^\pi = 1^-$ octupole vibration has been suggested to appear on top of the SD state in ^{40}Ca. For ^{48,50}S close to the neutron drip line, we have found that the low-lying state created by the excitation of a single neutron from a loosely bound low Ω level to a high Ω resonance level acquires an extremely strong octupole transition strength due to the spatially very extended structure of the particle-hole wave functions.

Acknowledgements

This work was done as a part of the Japan-US Cooperative Science Program "Mean-Field Approach to Collective Excitations in Unstable Medium-Mass and Heavy Nuclei" during the academic years 2003-2004, and we greatly appreciate useful discussions with the members of this project. This work was supported by the Grant-in-Aid for Scientific Research (No. 16540249) from the Japan Society for the Promotion of Science. We also thank the Yukawa Institute for Theoretical Physics at Kyoto University: Discussions during the YITP workshop YITP-W-05-01 on "New Developments in Nuclear Self-Consistent Mean-Field Theories" were useful to complete this work. The numerical calculations were performed

on the NEC SX-5 supercomputers at RCNP, Osaka University, and at Yukawa Institute for Theoretical Physics, Kyoto University.

A Explicit expressions of the RPA Hamiltonian

Here, using the notations of Ref. [63], we recapitulate the quantities appearing in the RPA Hamiltonian (19). More detailed expressions are given in Ref. [51].

The RPA Hamiltonian $h_{\rm RPA}^{(\pm)\lambda}$ is written

$$h_{\rm RPA}^{(\pm)\lambda}(\boldsymbol{r}\sigma\tau,\boldsymbol{r}\sigma'\tau') = \left[F_{00}^{(\pm)\lambda}(\boldsymbol{r})\delta_{\tau\tau'} + \sum_{t_3} F_{1t_3}^{(\pm)\lambda}(\boldsymbol{r})\tau_{\tau\tau'}^{t_3}\right]\delta_{\sigma\sigma'} + \left[\boldsymbol{G}_{00}^{(\pm)\lambda}(\boldsymbol{r})\delta_{\tau\tau'} + \sum_{t_3} \boldsymbol{G}_{1t_3}^{(\pm)\lambda}(\boldsymbol{r})\tau_{\tau\tau'}^{t_3}\right]\cdot\boldsymbol{\sigma}_{\sigma\sigma'}, \tag{22}$$

$$F_{tt_3}^{(\pm)\lambda} = -\nabla\cdot\left[M_{tt_3}^{(\pm)\lambda}\nabla\right] + U_{tt_3}^{(\pm)\lambda} - \frac{i}{2}\left[\nabla\cdot\boldsymbol{I}_{tt_3}^{(\pm)\lambda} + \boldsymbol{I}_{tt_3}^{(\pm)\lambda}\cdot\nabla\right] + U_{{\rm Coul},tt_3}^{(\pm)\lambda}\delta_{\pi\tau}, \tag{23}$$

$$\boldsymbol{G}_{tt_3}^{(\pm)\lambda} = -\sum_{\mu}\nabla_\mu\cdot\left[\boldsymbol{C}_{tt_3}^{(\pm)\lambda}\nabla_\mu\right] + \boldsymbol{\Sigma}_{tt_3}^{(\pm)\lambda} - \frac{i}{2}\sum_{\mu\nu}\left[\nabla_\mu B_{tt_3,\mu\nu}^{(\pm)\lambda} + B_{tt_3,\mu\nu}^{(\pm)\lambda}\nabla_\mu\right]\boldsymbol{e}_\nu. \tag{24}$$

The quantities, $M_{tt_3}^{(\pm)\lambda}, U_{tt_3}^{(\pm)\lambda}$, *etc.* appearing in the above expressions are obtained by the second derivative of the time-even and time-odd energy functionals, $\mathcal{E}^{\rm even}$ and $\mathcal{E}^{\rm odd}$, with respect to the local densities:

$$M_{tt_3}^{(\pm)\lambda} = \frac{\partial^2\mathcal{E}_t^{\rm even}}{\partial\tau_{tt_3}\partial\rho_{tt_3}}\rho_{tt_3}^{(\pm)\lambda}, \tag{25}$$

$$U_{00}^{(\pm)\lambda} = \frac{\partial}{\partial\rho_{00}}\left[\sum_{tt_3}\left(\frac{\partial\mathcal{E}_{\rm Sk}}{\partial\rho_{tt_3}}\rho_{tt_3}^{(\pm)\lambda} + \frac{\partial\mathcal{E}_t^{\rm odd}}{\partial\boldsymbol{s}_{tt_3}}\cdot\boldsymbol{s}_{tt_3}^{(\pm)\lambda}\right) + \frac{\partial\mathcal{E}_0^{\rm even}}{\partial\tau_{00}}\tau_{00}^{(\pm)\lambda} + \frac{\partial\mathcal{E}_0^{\rm even}}{\partial\boldsymbol{J}_{00}}\cdot\boldsymbol{J}_{00}^{(\pm)\lambda}\right] \tag{26}$$

$$U_{1t_3}^{(\pm)\lambda} = \frac{\partial}{\partial\rho_{1t_3}}\left[\frac{\partial\mathcal{E}_1^{\rm even}}{\partial\rho_{1t_3}}\rho_{1t_3}^{(\pm)\lambda} + \frac{\partial\mathcal{E}_1^{\rm even}}{\partial\tau_{1t_3}}\tau_{1t_3}^{(\pm)\lambda} + \frac{\partial\mathcal{E}_1^{\rm even}}{\partial\boldsymbol{J}_{1t_3}}\cdot\boldsymbol{J}_{1t_3}^{(\pm)\lambda} + \frac{\partial\mathcal{E}_1^{\rm even}}{\partial\rho_{00}}\rho_{00}^{(\pm)\lambda}\right], \tag{27}$$

$$B_{tt_3,\mu\nu}^{(\pm)\lambda} = \frac{\partial}{\partial J_{tt_3,\mu\nu}}\left[\frac{\partial\mathcal{E}_t^{\rm even}}{\partial J_{tt_3,\mu\nu}}J_{tt_3,\mu\nu}^{(\pm)\lambda} + \frac{\partial\mathcal{E}_t^{\rm even}}{\partial\rho_{tt_3}}\rho_{tt_3}^{(\pm)\lambda}\right], \tag{28}$$

$$\boldsymbol{C}_{tt_3}^{(\pm)\lambda} = \frac{\partial^2\mathcal{E}_t^{\rm odd}}{\partial\boldsymbol{T}_{tt_3}\partial\boldsymbol{s}_{tt_3}}\cdot\boldsymbol{s}_{tt_3}^{(\pm)\lambda}, \tag{29}$$

$$\boldsymbol{\Sigma}_{tt_3}^{(\pm)\lambda} = \frac{\partial}{\partial\boldsymbol{s}_{tt_3}}\left[\frac{\partial\mathcal{E}_t^{\rm odd}}{\partial\boldsymbol{s}_{tt_3}}\cdot\boldsymbol{s}_{tt_3}^{(\pm)\lambda} + \frac{\partial\mathcal{E}_t^{\rm odd}}{\partial\boldsymbol{T}_{tt_3}}\cdot\boldsymbol{T}_{tt_3}^{(\pm)\lambda} + \frac{\partial\mathcal{E}_t^{\rm odd}}{\partial\boldsymbol{j}_{tt_3}}\cdot\boldsymbol{j}_{tt_3}^{(\pm)\lambda} + \frac{\partial\mathcal{E}_t^{\rm odd}}{\partial\rho_{00}}\rho_{00}^{(\pm)\lambda}\right], \tag{30}$$

$$\boldsymbol{I}_{tt_3}^{(\pm)\lambda} = \frac{\partial}{\partial\boldsymbol{j}_{tt_3}}\left[\frac{\partial\mathcal{E}_t^{\rm odd}}{\partial\boldsymbol{j}_{tt_3}}\cdot\boldsymbol{j}_{tt_3}^{(\pm)\lambda} + \frac{\partial\mathcal{E}_t^{\rm odd}}{\partial\boldsymbol{s}_{tt_3}}\cdot\boldsymbol{s}_{tt_3}^{(\pm)\lambda}\right], \tag{31}$$

$$U_{{\rm Coul},tt_3}^{(\pm)\lambda} = \frac{\partial}{\partial\rho_{tt_3}}\left[\frac{\partial\mathcal{E}_{\rm Coul}}{\partial\rho_{00}}\rho_{00}^{(\pm)\lambda} + \frac{\partial\mathcal{E}_{\rm Coul}}{\partial\rho_{10}}\rho_{10}^{(\pm)\lambda}\right]. \tag{32}$$

The local transition densities $\rho_{tt_3}^{(\pm)\lambda}$, the local transition spin densities $\boldsymbol{s}_{tt_3}^{(\pm)\lambda}$, the local transition kinetic energy densities $\tau_{tt_3}^{(\pm)\lambda}$, the local transition kinetic spin densities $\boldsymbol{T}_{tt_3}^{(\pm)\lambda}$, the local transition current densities $\boldsymbol{j}_{tt_3}^{(\pm)\lambda}$, the local transition spin-orbit current tensors $J_{tt_3,\mu\nu}^{(\pm)\lambda}$ are given by

$$\rho_{tt_3}^{(\pm)\lambda}(\boldsymbol{r}) = \rho_{tt_3}^{(\pm)\lambda}(\boldsymbol{r},\boldsymbol{r}), \tag{33}$$

$$
\begin{aligned}
\boldsymbol{s}^{(\pm)\lambda}_{tt_3}(\boldsymbol{r}) &= \boldsymbol{s}^{(\pm)\lambda}_{tt_3}(\boldsymbol{r},\boldsymbol{r}), && (34)\\
\tau^{(\pm)\lambda}_{tt_3}(\boldsymbol{r}) &= \nabla\cdot\nabla'\rho^{(\pm)\lambda}_{tt_3}(\boldsymbol{r},\boldsymbol{r}')\Big|_{\boldsymbol{r}=\boldsymbol{r}'}, && (35)\\
\boldsymbol{T}^{(\pm)\lambda}_{tt_3}(\boldsymbol{r}) &= \nabla\cdot\nabla'\boldsymbol{s}^{(\pm)\lambda}_{tt_3}(\boldsymbol{r},\boldsymbol{r}')\Big|_{\boldsymbol{r}=\boldsymbol{r}'}, && (36)\\
\boldsymbol{j}^{(\pm)\lambda}_{tt_3}(\boldsymbol{r}) &= -\frac{i}{2}\left(\nabla-\nabla'\right)\rho^{(\pm)\lambda}_{tt_3}(\boldsymbol{r},\boldsymbol{r}')\Big|_{\boldsymbol{r}=\boldsymbol{r}'}, && (37)\\
J^{(\pm)\lambda}_{tt_3,\mu\nu}(\boldsymbol{r}) &= -\frac{i}{2}\left(\nabla-\nabla'\right)_\mu \boldsymbol{s}^{(\pm)\lambda}_{tt_3,\nu}(\boldsymbol{r},\boldsymbol{r}')\Big|_{\boldsymbol{r}=\boldsymbol{r}'}. && (38)
\end{aligned}
$$

The local transition spin-orbit currents $\boldsymbol{J}^{(\pm)\lambda}_{tt_3}$ are defined by

$$
\boldsymbol{J}^{(\pm)\lambda}_{tt_3} = \sum_{\mu\nu\omega}\epsilon_{\mu\nu\omega}J^{(\pm)\lambda}_{tt_3,\nu\nu}\boldsymbol{e}_\omega, \qquad (39)
$$

where $\epsilon_{\mu\nu\omega}$ is the Levi-Civita symbol and $\boldsymbol{e}_\omega$ is the unit vector in the ω-direction. The scalar transition densities $\rho^{(\pm)\lambda}_{tt_3}(\boldsymbol{r},\boldsymbol{r}')$ and the vector transition densities $\boldsymbol{s}^{(\pm)\lambda}_{tt_3}(\boldsymbol{r},\boldsymbol{r}')$ appearing in the above equations are defined by decomposing the transition density matrix $\rho^{(\pm)\lambda}(x,x') = \rho^{(\pm)\lambda}(\boldsymbol{r}\sigma\tau,\boldsymbol{r}'\sigma'\tau')$ into the spin-isospin channels:

$$
\begin{aligned}
\rho^{(\pm)\lambda}(\boldsymbol{r}\sigma\tau,\boldsymbol{r}'\sigma'\tau') = \quad & \frac{1}{4}\Big[\rho^{(\pm)\lambda}_{00}(\boldsymbol{r},\boldsymbol{r}')\delta_{\sigma\sigma'}\delta_{\tau\tau'} + \boldsymbol{s}^{(\pm)\lambda}_{00}(\boldsymbol{r},\boldsymbol{r}')\cdot\boldsymbol{\sigma}_{\sigma\sigma'}\delta_{\tau\tau'}\\
& +\delta_{\sigma\sigma'}\sum_{t_3=-1}^{1}\rho^{(\pm)\lambda}_{1t_3}(\boldsymbol{r},\boldsymbol{r}')\tau^{t_3}_{\tau\tau'} + \sum_{t_3=-1}^{1}\boldsymbol{s}^{(\pm)\lambda}_{1t_3}(\boldsymbol{r},\boldsymbol{r}')\cdot\boldsymbol{\sigma}_{\sigma\sigma'}\tau^{t_3}_{\tau\tau'}\Big]. \qquad (40)
\end{aligned}
$$

In the above expressions, the charge-exchange $t_3 = \pm 1$ components are included for completeness, although they do not contribute to the excitation modes considered in this paper.

References

[1] P.J. Nolan and P.J. Twin, Annu. Rev. Nucl. Part. Sci. 38 (1988) 533.

[2] S. Åberg, H. Flocard and W. Nazarewicz, Annu. Rev. Nucl. Part. Sci. 40 (1990) 439.

[3] R.V.F. Janssens and T.L. Khoo, Annu. Rev. Nucl. Part. Sci. 41 (1991) 321.

[4] C. Baktash, B. Haas and W. Nazaerewicz, Annu. Rev. Nucl. Part. Sci. 45 (1995) 485.

[5] C. Baktash, Prog. Part. Nucl. Phys. 38 (1997) 291.

[6] J. Dobaczewski, Proc. Int. Conf. on Nuclear Structure '98 (AIP conference proceedings 481), ed. C. Baktash, p. 315.

[7] J. Dudek, T.R. Werner and Z. Szymanski, Phys. Lett. B 248 (1990) 235.

[8] J. Skalski, Phys. Lett. B 274 (1992) 1.

[9] P.A. Butler and W. Nazarewicz, Rev. Mod. Phys. 68 (1996) 349.

[10] S. Mizutori, Y.R. Shimizu, and K. Matsuyanagi, Prog. Theor. Phys. 85 (1991) 559; *ibid.* 86 (1991) 131.

[11] S. Mizutori, T. Nakatsukasa, K. Arita, Y.R. Shimizu, and K. Matsuyanagi, Nucl. Phys. A 557 (1993) 125c.

[12] T. Nakatsukasa, K. Matsuyanagi, S. Mizutori, Y.R. Shimizu, Phys. Rev. C 53 (1996) 2213.

[13] A. Korichi *et al.*, Phys. Rev. Lett. 86 (2001) 2746, D. Rossbach *et al.*, Phys. Lett. B 513 (2001) 9.

[14] T. Lauritsen *et al.*, Phys. Rev. Lett. 89 (2002) 282501.

[15] C.E. Svensson *et al.*, Phys. Rev. Lett. 85 (2000) 2693.

[16] C.E. Svensson *et al.*, Phys. Rev. C 63 (2001) 061301(R).

[17] C.E. Svensson *et al.*, Nucl. Phys. A 682 (2001) 1c.

[18] E. Ideguchi *et al.*, Phys. Rev. Lett. 87 (2001), 222501.

[19] C.J. Chiara *et al.*, Phys. Rev. C 67 (2003), 041303.

[20] C.D. O'Leary, M.A. Bentley, B.A. Brown, D.E. Appelbe, R.A. Bark, D.M. Cullen, S. Ertürk, A. Maj and A.C. Merchant, Phys. Rev. C 61 (2000) 064314.

[21] T. Inakura, S. Mizutori, M. Yamagami, and K. Matsuyanagi, Nucl. Phys. A 710 (2002) 261.

[22] R.K. Sheline, I. Ragnarsson and S.G. Nilsson, Phys. Lett. B 41 (1972) 115.

[23] G. Leander and S.E. Larsson, Nucl. Phys. A 239 (1975) 93.

[24] I. Ragnarsson, S.G. Nilsson and R.K. Sheline, Phys. Rep. 45 (1978) 1.

[25] T. Bengtsson, M.E. Faber, G. Leander, P. Möller, M. Ploszajczak, I Ragnarsson and S. Åberg, Phys. Scr. 24 (1981) 200.

[26] M. Girod and B. Grammaticos, Phys. Rev. C 27 (1983) 2317.

[27] M. Yamagami and K. Matsuyanagi, Nucl. Phys. A 672 (2000) 123.

[28] H. Molique, J. Dobaczewski, J. Dudek, Phys. Rev. C 61 (2000) 044304.

[29] R.R. Rodriguez-Guzmán, J.L. Egido and L.M. Robeldo, Phys. Rev. C 62 (2000) 054308.

[30] T. Tanaka, R.G. Nazmitdinov and K. Iwasawa, Phys. Rev. C 63 (2001) 034309.

[31] A.V. Afanasjev, P. Ring and I. Ragnarsson, in: D. Rudolph, M. Hellström (Eds.), Proc. Int. Workshop on Selected Topics on $N{=}Z$ Nuclei (PINGST 2000), Lund, Sweden, June 6-10, 2000, p.183.

[32] C.E. Svensson *et al.*, Phys. Rev. Lett. 82 (1999) 3400.

[33] C.E. Svensson *et al.*, Phys. Rev. Lett. 79 (1997) 1233.

[34] T.R. Werner, J.A. Sheikh, W. Nazarewicz, M.R. Strayer, A.S. Umar and M. Misu, Phys. Lett. B 333 (1994) 303.

[35] T.R. Werner, J.A. Sheikh, M. Misu, W. Nazarewicz, J. Rikovska, K. Heeger, A.S. Umar and M.R. Strayer, Nucl. Phys. A 597 (1996) 327.

[36] T. Inakura, S. Mizutori, M. Yamagami, and K. Matsuyanagi, Nucl. Phys. A 728 (2003) 52.

[37] G. F. Bertsch and S. F. Tsai, Phys. Rep. 18 (1975) 125.

[38] S. Shlomo and G. F. Bertsch, Nucl. Phys. A 243 (1975) 507.

[39] I. Hamamoto, H. Sagawa, and X. Z. Zhang, Nucl. Phys. A 648 (1999) 203.

[40] H. Sagawa, Prog. Theor. Phys. Suppl. 142 (2001) 1.

[41] M. Matsuo, Nucl. Phys. A 696 (2001) 371.

[42] E. Khan, N. Sandulescu, M. Grasso, and Nguyen Van Giai, Phys. Rev. C 66 (2002) 024309.

[43] M. Yamagami and Nguyen Van Giai, Phys. Rev. C 69 (2004) 034301.

[44] J. Terasaki, J. Engel, M. Bender, J. Dobaczewski, W. Nazarewicz, and M. Stoitsov, Phys. Rev. C 71 (2005) 034310.

[45] D. Vretenar, N. Paar, P. Ring and G. A. Lalazissis, Nucl. Phys. A 692 (2001) 496.

[46] N. Paar, T. Niksic, D. Vretenar and P. Ring, Phys. Lett. B 606 (2005) 288.

[47] T. Nakatsukasa and K. Yabana, Phys. Rev. C 71 (2005) 024301.

[48] R.H. Lemmer and M. Vénéroni, Phys. Rev. 170 (1968) 883.

[49] G.F. Bertsch, Prog. Theor. Phys. Suppl. Nos. 74/75 (1983) 115.

[50] A. Muta, J-I. Iwata, Y. Hashimoto, and K. Yabana, Prog. Theor. Phys. 108 (2002) 1065.

[51] H. Imagawa, Doctor Thesis, University of Tsukuba, April 2003.

[52] H. Imagawa and Y. Hashimoto, Phys. Rev. C 67 (2003) 037302.

[53] H. Imagawa and Y. Hashimoto, in preparation.

[54] T. Inakura, M. Yamagami, K. Matsuyanagi, S. Mizutori, H. Imagawa and Y. Hashimoto, *Proceedings of the 10th Marie and Pierre Curie Nuclear Physics Workshop*, September 24-28, 2003, Kazimierz Dolny, Poland, [Int. J. Mod. Phys. **E 13** (2004) 157].

[55] T. Inakura, H. Imagawa, Y. Hashimoto, M. Yamagami, S. Mizutori and K. Matsuyanagi, *Proceedings of the Fourth International Conference on Exotic Nuclei and Atomic Masses*, September 12-16, 2004, Pine Mountain, [Eur. Phys. J. **A** direct (2005)].

[56] D. Baye and P.-H. Heenen, J. Phys. A 19 (1986) 2041.

[57] M. Beiner, H. Flocard, Nguyen van Giai, and P. Quentin, Nucl. Phys. A 238 (1975) 29.

[58] J. Bartel, P. Quentin, M. Brack, C. Guet, and H.B. Håkansson, Nucl. Phys. A 386 (1982) 79.

[59] E. Chanbanat, P. Bonche, P. Haensel, J. Mayer, and R. Schaeffer, Nucl. Phys. A 627 (1997) 710.

[60] K. Yoshida, M. Yamagami and K. Matsuyanagi, Prog. Theor. Phys. 113 (2005) 1251.

[61] A. Bohr and B.R. Mottelson, Nuclear Structure, Vol. 2, Benjamin, Reading, MA, 1975.

[62] M. Yamagami, e-print, arXiv:nucl-th/0504059.

[63] M. Bender, J. Dobaczewski, J. Engel, and W. Nazarewicz, Phys. Rev. C 65 (2002) 054322.

Table 1: Classification of octupole and dipole operators according to the parity quantum numbers with respect to reflections about the (y,z)-, (z,x)- and (x,y)-planes.

symmetry	octupole	dipole
$(-,+,+)$	$Q_{31}^{(+)},\ Q_{33}^{(+)}$	x
$(+,-,+)$	$Q_{31}^{(+)},\ Q_{33}^{(+)}$	y
$(+,+,-)$	$Q_{30},\ Q_{32}^{(+)}$	z
$(-,-,-)$	$Q_{32}^{(-)}$	none

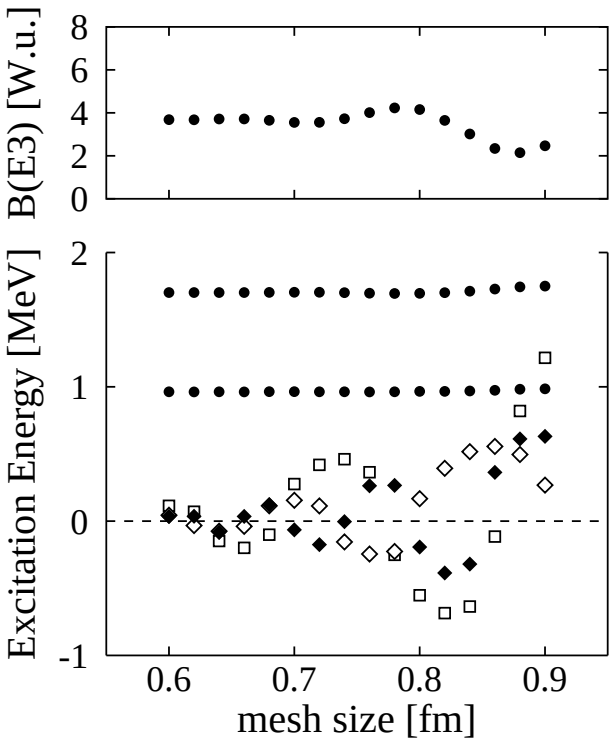

Figure 1: Low-energy solutions of the RPA for negative-parity excitations on the SD ground state in ^{40}Ca, plotted as functions of the mesh spacing used in the SHF+RPA calculation with the SIII interaction. *Lower part*: Energies of the spurious center of mass modes belonging to the $(-,+,+)$, $(+,-,+)$ and $(+,+,-)$ sectors are plotted with open diamonds, filled diamonds, and open squares, respectively. When their excitation energies, $\hbar\omega_\lambda$, take imaginary values, the $-|\omega_\lambda|$ values are plotted for convenience of presentation. The filled circles at about 1.0 and 1.7 MeV indicate the lowest physical excitations in the $(-,+,+)$ and $(+,-,+)$ sectors, respectively. *Upper part*: Transition strengths for the lowest physical excitation at about 1.7 MeV in the $(+,-,+)$ sector, plotted as a function of mesh spacing.

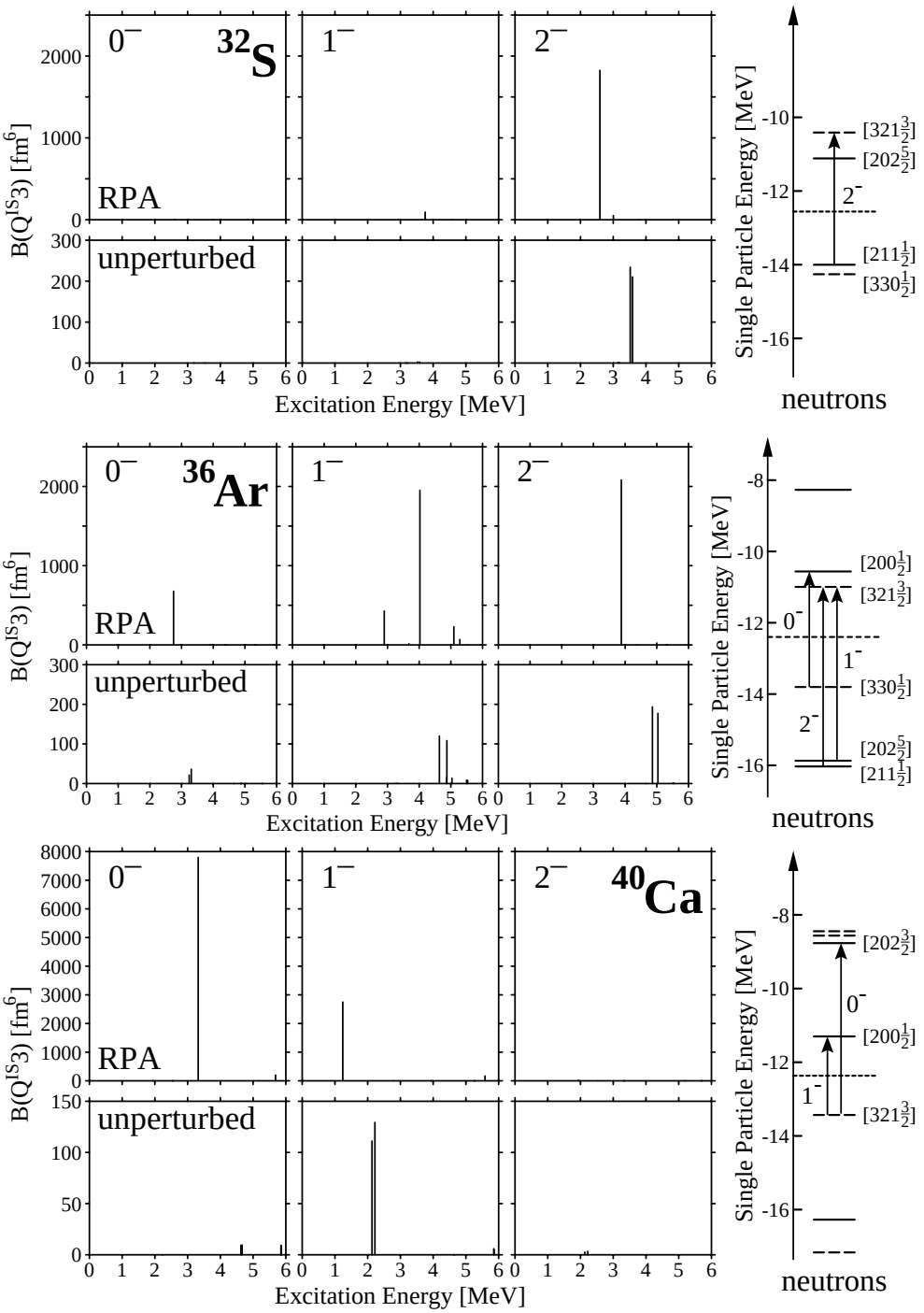

Figure 2: Isoscalar octupole transition strengths for $K^\pi = 0^-, 1^-$ and 2^- excitations on the SD states in (a) ^{32}S, (b) ^{36}Ar, and (c) ^{40}Ca, obtained by the SHF-RPA calculation with the SIII interaction. The unit is fm^6. For comparison with the RPA strengths, unperturbed particle-hole strengths are also shown in the lower panels for each nucleus. There are no significant strengths for $K^\pi = 3^-$ excitations values in this low-energy region, so that they are not shown. Some particle-hole excitations of neutrons near the Fermi surface are drawn by arrows with their K^π values in the rightmost part for each nucleus. We have similar excitations also for protons. The solid, dashed, and dotted lines indicate positive-parity levels, negative-parity levels, and the Fermi surface, respectively. The asymptotic quantum numbers $[Nn_z\Lambda\Omega]$ are indicated for pertinent levels.

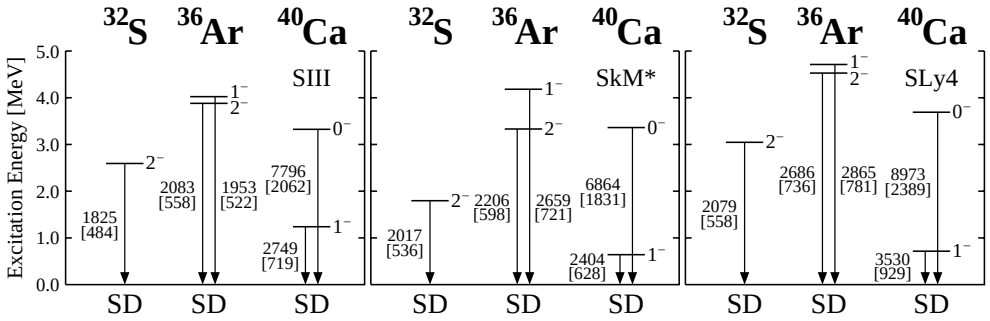

Figure 3: Comparison of the SHF-RPA calculations with the SIII, SkM* and SLy4 interactions for collective octupole excitations on the SD states in ^{32}S, ^{36}Ar, and ^{40}Ca. Only collective excitations having $B(Q^{\rm IS}3)$ greater than 10 W.u. are displayed here (see Fig. 2 for other excitations having smaller strengths). The numbers on the right-hand sides of individual levels indicate the K quantum numbers. The numbers beside the arrows indicate the intrinsic transition matrix elements squared of the isoscalar octupole operator, $B(Q^{\rm IS}3)$, in units of fm^6. Those for the electric octupole operator, $B(E3)$, are also given in brackets in units of e^2fm^6.

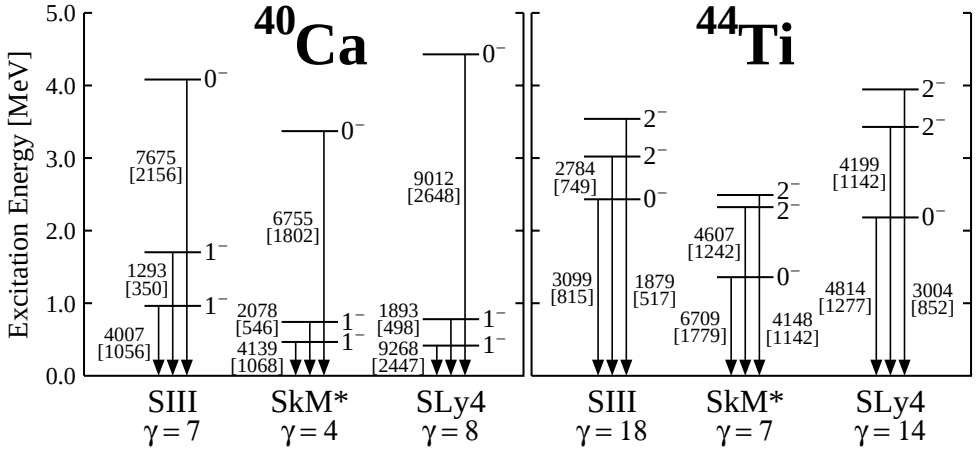

Figure 4: Low-frequency collective octupole excitations on the SD states in ^{40}Ca and ^{44}Ti, obtained by the SHF-RPA calculation taking into account the triaxial deformation of the mean field. Only collective excitations having $B(Q^{\rm IS}3)$ greater than 10 W.u. are displayed here. The numbers on the right-hand sides of individual levels indicate the approximate K quantum numbers, The numbers beside the arrows indicate the intrinsic transition matrix elements squared of the isoscalar octupole operator, $B(Q^{\rm IS}3)$, in units of fm^6. Those for the electric octupole operator, $B(E3)$, are also given in brackets in units of e^2fm^6. The Skyrme interaction used and the triaxial deformation γ of the mean field are indicated at the bottom.

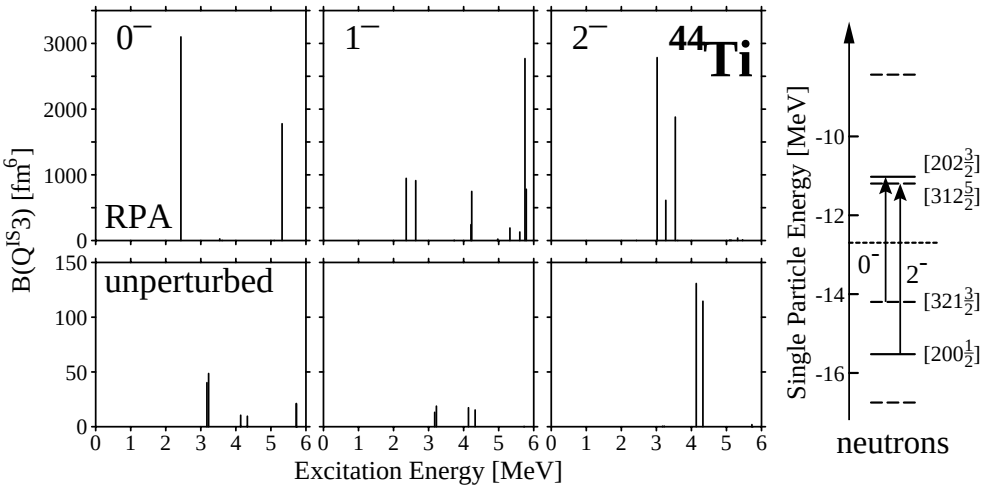

Figure 5: The same as Fig. 2, but for octupole excitations on the triaxial SD state in ^{44}Ti. Note that, due to the triaxial deformation, K is not a good number for single-particle levels. The asymptotic quantum numbers $[Nn_z\Lambda\Omega]$ beside the pertinent levels in the rightmost figure merely indicate their main components.

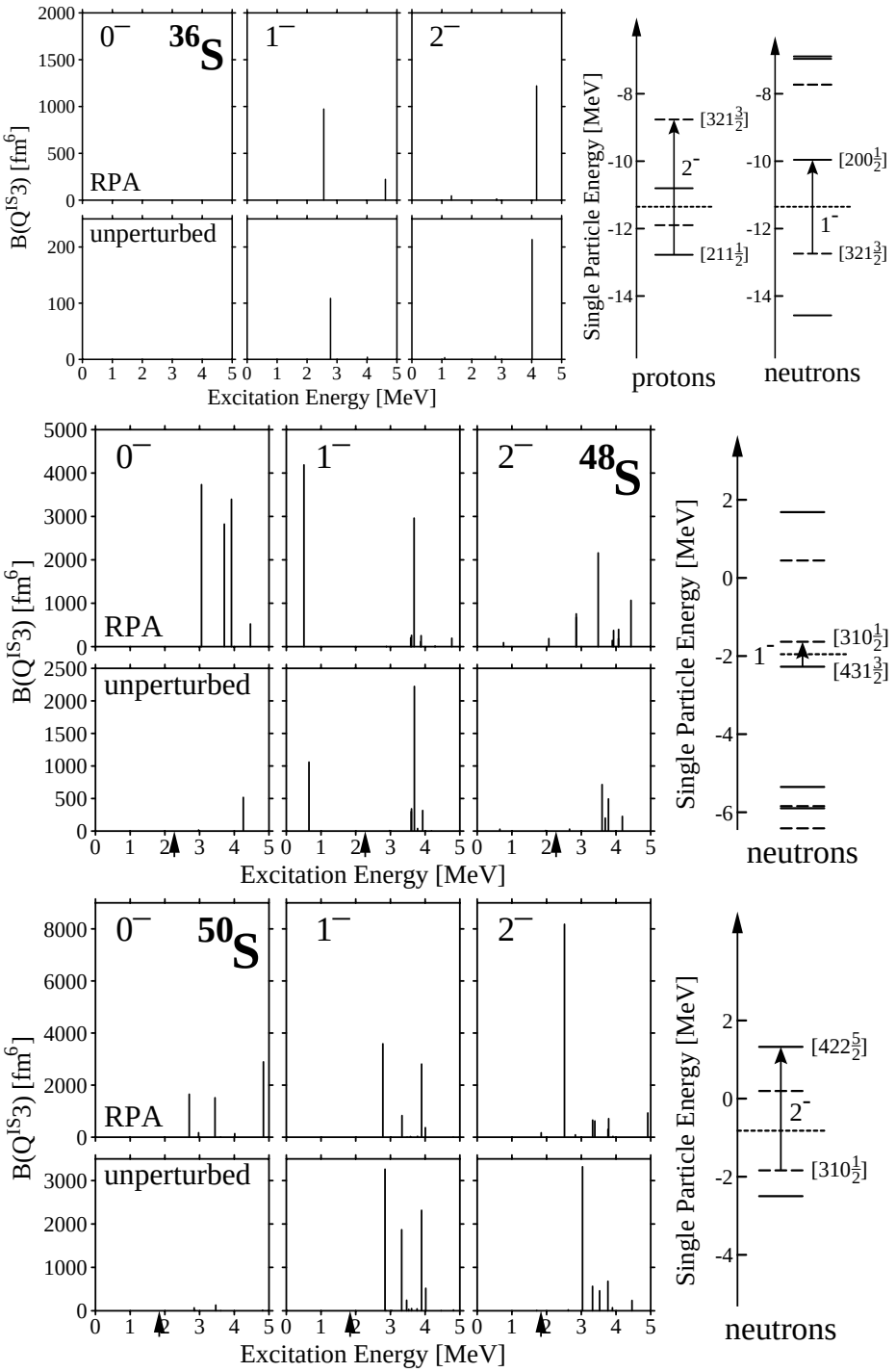

Figure 6: Isoscalar octupole transition strengths for $K^\pi = 0^-, 1^-$ and 2^- excitations on the SD states in (a) ^{36}S, (b) ^{48}S, and (c) ^{50}S, obtained by the SHF-RPA calculation with the SIII interaction. The unit is fm^6. For comparison with the RPA strengths, unperturbed particle-hole strengths are also shown in the lower panels for each nucleus. The arrows indicate the threshold energies for neutron emission. There are no significant strengths for $K^\pi = 3^-$ excitations in this low-energy region, so that they are not shown. Some particle-hole excitations near the Fermi surface are drawn by arrows with their K^π values in the rightmost part for each nucleus. The solid, dashed, and dotted lines indicate the positive-parity levels, negative-parity levels, and the Fermi surface, respectively. The asymptotic quantum numbers $[Nn_z\Lambda\Omega]$ are indicated for pertinent levels. For the positive energy region, only the discretized continuum levels possessing resonance character are drawn.

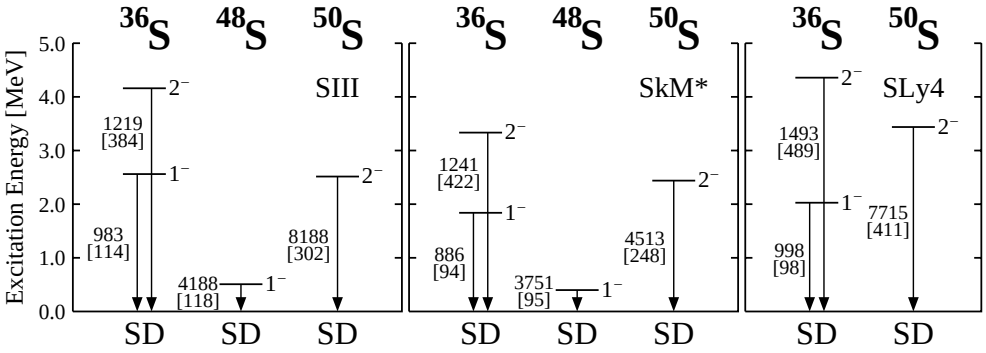

Figure 7: Comparison of the SHF-RPA calculations with the SIII, SkM* and SLy4 interactions for low-frequency $K^\pi = 1^-$ and 2^- excitations on the SD states in ^{36,48,50}S. For SLy4, the SD local minimum does not appear in ^{48}S. Only excitations having $B(Q^{\rm IS}3)$ greater than 10 W.u. are displayed here (see Fig. 6 for other excitations having smaller strengths). The numbers on the right-hand sides of individual levels indicate the K quantum numbers. The numbers beside the arrows indicate the intrinsic transition matrix elements squared of the isoscalar octupole operator, $B(Q^{\rm IS}3)$, in units of fm^6. Those for the electric octupole operator, $B(E3)$, are also given in brackets in units of e^2fm^6.